Journal of
Materials Chemistry C

Materials for optical, magnetic and electronic devices
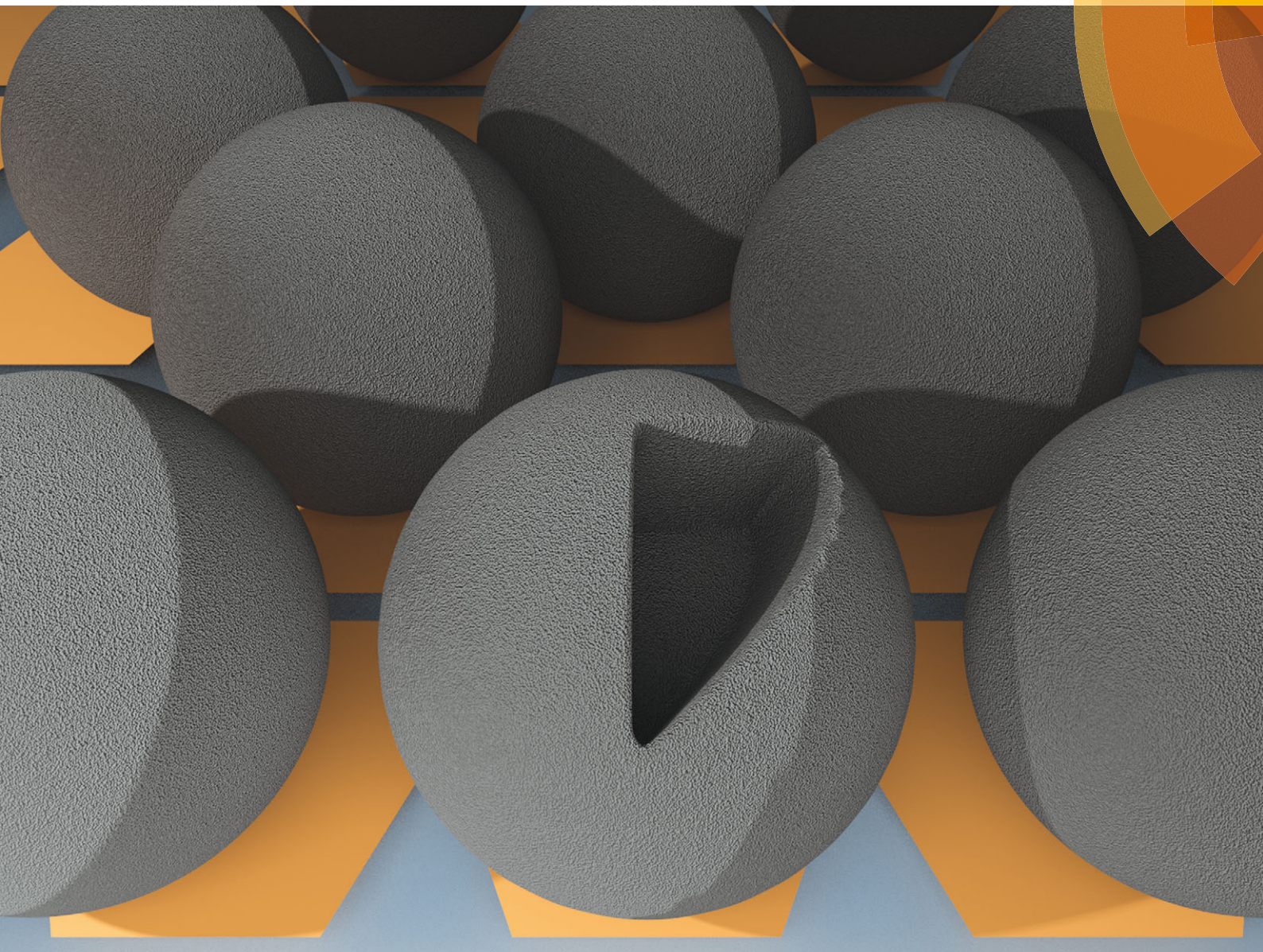
PAPER
Gonzalo Abellán, Eugenio Coronado *et al.*
CVD synthesis of carbon spheres using NiFe-LDHs as catalytic precursors:
structural, electrochemical and magnetoresistive properties

175 YEARS

CVD synthesis of carbon spheres using NiFe-LDHs as catalytic precursors: structural, electrochemical and magnetoresistive properties†

Jose A. Carrasco,[a] Helena Prima-Garcia,[a] Jorge Romero,[a] Jesús Hernández-Saz,[b] Sergio I. Molina,[b] Gonzalo Abellán*[ac] and Eugenio Coronado*[a]

The gram-scale synthesis of carbon spheres with a diameter of *ca.* 740 nm has been achieved by means of a chemical vapour deposition method using NiFe-layered double hydroxides as a solid catalytic precursor. The presence of the catalyst ($FeNi_3$) allows controlling the final size distribution, resulting in a monodisperse sample. Their structural properties exhibited a high degree of graphitization according to their I_D/I_G ratio. In addition, their morphological features were unveiled by FIB-SEM and HRTEM, showing that they are formed by solid inner cores, and presenting labile chain-like structures due to accretion procedures. The solution and posterior sonication of the samples in toluene gave rise to the well-defined isolated spheres. The textural and electrochemical properties of the spheres have been tested showing non-mesoporous structures with a good behaviour as electrode materials for supercapacitors due to the presence of redox functionalities on their surface. Finally, magneto-transport measurements have been carried out, demonstrating semiconductor behaviour, as well as a positive magnetoresistance effect (*ca.* 72%) for the lowest studied temperature (2 K).

1. Introduction

Since the discovery of fullerenes (C_{60}) by Kroto *et al.* in 1985,[1] many studies have been published in the field of the so-called carbon nanoforms (CNF). These carbon-based materials include a wide variety of sizes and shapes ranging from C_{60} to metallofullerenes, carbon fibers, nanotubes (single-wall, multi-wall…), nano-onions, nanohorns, nanobuds, spheres or graphene, among others.[2] The interest in different synthetic carbon allotropes relies on their outstanding properties and applications, as recently highlighted by the ubiquitous graphene. Among this family, spherical carbon structures like C_{60}, or carbon nano-onions have attracted increasing attention in the last few years. One of these forms are carbon spheres (CS), formerly known as carbon blacks.[3] The curved structure of CS is a consequence of the presence of pentagonal and heptagonal rings within the hexagonal framework of carbon, allowing the system to adopt their characteristic morphology.[4]

Carbon spheres can be classified according to different parameters, like their size, nanometric texture or internal structure.[5–8] Recently, Deshmukh *et al.* reviewed different techniques employed for the synthesis of CS, pointing out chemical vapour deposition (CVD) as one of the most versatile synthetic approaches.[9]

These carbonaceous forms show a wide range of potential applications due to their thermal stability, electronic properties, high surface area or low density. Furthermore, their unclosed graphitic flakes give rise to dangling bonds throughout the surface of the spheres, increasing their reactivity and boosting their applicability in adsorption, lubricants, tribological coatings, catalysis, batteries, supercapacitors or fuel cells among others.[10–15] Conversely, when it comes to their transport and magnetic properties, the list of examples is very scarce,[16,17] despite their potential for use as electronically active reinforcing agents of functional composites.[18,19] Indeed, the recent discovery of organic magnetoresistance (OMAR) in graphene and other related nanocarbons has significantly attracted increasing attention to these systems, as they are promising materials for flexible, low-cost and transparent electronics.[20–25] Therefore, the cost-effective production of magnetoresistive CS is of great interest in the development of new hybrid composites and functional polymers.

Herein, we have synthesized monodisperse carbon spheres in a gram-scale by means of a CVD procedure using NiFe-layered

[a] Instituto de Ciencia Molecular (ICMol), Universidad de Valencia, Catedrático José Beltrán 2, 46980, Paterna, Valencia, Spain. E-mail: eugenio.coronado@uv.es; Fax: +34 96 354 3273; Tel: +34 96 354 4415

[b] Departamento de Ciencia de los Materiales e Ingeniería Metalúrgica y Química Inorgánica, IMEYMAT, Universidad de Cádiz, 11510 Puerto Real, Cádiz, Spain

[c] Department of Chemistry and Pharmacy and Institute of Advanced Materials and Processes (ZMP), University Erlangen-Nürnberg, Henkestr. 42, 91054 Erlangen and Dr.-Mack Str. 81, 90762 Fürth, Germany. E-mail: gonzalo.abellan@fau.de; Fax: +49 911 65078 65015; Tel: +49 911 65078 65031

† Electronic supplementary information (ESI) available. See DOI: 10.1039/c5tc02861b

double hydroxides (LDHs) as catalytic precursors.[26] The NiFe-LDH materials have demonstrated their utility as catalysts in the low-temperature synthesis of several carbon nanoforms, including carbon nano-onions,[27] bamboo-like carbon nanotubes[28] or even graphene – when they are used as precursors for the preparation of hybrid $FeNi_3$–graphene nanocomposites.[28–30]

We have thoroughly characterized the as-obtained spheres by means of XRD, Raman, FT-IR, TG, FESEM, FIB-SEM, HRTEM, DLS, N_2 isotherms, XPS and Electrochemistry. Furthermore, their magneto-transport properties revealed a semiconducting behaviour with an intrinsic large MR of ca. 72%.

2. Experimental methods

2.1. Chemicals

All chemical reagents $Ni(NO_3)_2 \cdot 6H_2O$ (Aldrich); $Fe(NO_3)_3 \cdot 9H_2O$ (Sigma-Aldrich); triethanolamine (TEA), $C_6H_{15}NO_3$ (Sigma-Aldrich); urea, $CO(NH_2)_2$ (Fluka) and ethanol absolute (Panreac, 99.9%) were used as received without further purification. Ultrapure water was obtained from Millipore Milli-Q equipment. N_2, H_2/Ar (10%) and ethylene (C_2H_4) were purchased from Linde Material Handling.

2.2. Synthesis of NiFe-CO₃ LDHs

NiFe-CO₃ LDHs were synthesized following a modified homogeneous precipitation method by using urea and TEA as an ammonium releasing reagent (ARR) and a chelating agent, respectively.[31]

In a typical synthesis, the nitrate salts of the metals were dissolved in 50 mL of deionized pure water together with TEA, in order to reach a total metal cation concentration of 20 mM in the final solution, with a Ni : Fe ratio of 3 : 1 ($x = 0.25$, with $x = [Fe^{3+}]/([Fe^{3+}] + [Ni^{2+}])$), and a concentration of TEA equimolar with the iron concentration (5 mM). Next, 50 mL of aqueous solution of urea (35 mM) were added. The excess of urea was fixed to be 1.75 times the total metal concentration. The resulting dark brown mixture was placed in a 125 cm³ stainless steel Teflon-lined autoclave and heated up to 150 °C in a previously heated oven. After 48 h, the autoclave was left to cool down at room temperature and the final yellowish fine powder was filtered and dried under a vacuum. The pH value of the remaining solution was found to be around 8.

2.3. Synthesis of carbon spheres

Carbon spheres were synthesized by means of a chemical vapour deposition process (CVD). In a typical procedure, 25 mg of NiFe-LDHs were placed at the centre of a horizontal quartz tube, which was inserted into a tubular furnace at atmospheric pressure. The furnace was heated under flowing N_2 (100 mL min⁻¹) up to 900 °C at a 5 °C min⁻¹ scan rate. When the temperature was reached, reduction with H_2 (50 mL min⁻¹, mixture of H_2 10% in Ar) was performed for 5 min before switching the gas for the carbon source, ethylene (C_2H_4, 100 mL min⁻¹), during 60 more min at 900 °C. Then, the furnace was cooled to room temperature under N_2 protection, and the sample was collected from the quartz tube. Control experiments in the absence of

NiFe-LDHs were also carried out under the same experimental conditions.

2.4. Thermal treatment

The as-synthesized carbon spheres were annealed at 800 °C in order to eliminate organic impurities. In a typical procedure, the sample was placed in a holder at the centre of a horizontal quartz tube inserted into a furnace at atmospheric pressure. The furnace was heated up to 800 °C under a N_2 atmosphere (100 mL min⁻¹) at a 2 °C min⁻¹ scan rate. When the temperature was reached, the system was cooled to room temperature under N_2 protection. Finally, the annealed spheres were collected from the holder.

2.5. Physical characterization

X-ray powder diffraction (XRPD) patterns were obtained using a PANalytical Empyrean X-ray powder diffractometer under copper radiation (Cu-Kα = 1.54178 Å). Samples were mounted on a flat sample plate. Profiles were collected in the $2.5° < 2\theta < 90°$ range with a step size of 0.05°. Raman measurements (Jobin-Yvon LabRam HR 800 Raman Microscope) were carried out at room temperature with the 532 nm line of an Ar ion laser as an excitation source. The morphology of spheres was studied by means of field emission scanning electron microscopy (FESEM) performed on a Hitachi S-4800 microscope operating at an accelerating voltage of 20 kV over metallized samples with a mixture of gold and palladium for 30 s. FEI dual-beam FIB-SEM Quanta 200 3D equipment operating at 30 kV was used to mill the spheres and observe their inner structure and prepare lamellae by using an in situ lift-out method.[32] High-resolution transmission electron microscopy (HRTEM) studies were carried out on Tecnai G2 F20 and Jeol 2100 microscopes operating at 200 kV. Samples were prepared by dipping a sonicated suspension of the sample in toluene on a carbon-coated copper grid. Metallic atomic composition of bulk samples was determined by means of electron probe microanalysis (EPMA) performed on a Philips SEM-XL30 equipped with an EDAX microprobe. Carbon, nitrogen and hydrogen contents were determined by microanalytical procedures by using a LECO CHNS. Infrared spectra were recorded on a FT-IR Nicolet 5700 spectrometer in the 4000–400 cm⁻¹ range using powdered samples diluted in KBr pellets. Thermogravimetric analysis of the compounds were carried out using a Mettler Toledo TGA/SDTA 851 apparatus in the 25–800 °C temperature range at a 10 °C min⁻¹ scan rate and under an air flow of 30 mL min⁻¹. The porous texture was characterized by N_2 adsorption at 77 K in an AUTOSORB-6 apparatus. The samples were previously degassed for 4 h at 523 K and 5×10^{-5} bar. Dynamic light scattering (DLS) measurements were recorded at 25 °C using a Zetasizer Nano ZS instrument (Malvern Instrument Ltd) on a freshly prepared sample (1 mg of CS in 10 mL of toluene and sonicated for 30 min). The electrical conductivity and magneto-resistance measurements were carried out by using a standard four-probe contact method with Pt wire in a physical property measurement system (PPMS-9) by Quantum Design. The resistivity data were taken from 300 to 2 K and from 0 to 8 T, with Keithley 2450 as a current source and a

Keitley 6514 as an electrometer. The measurements were performed in a pressed pellet of the CS with a size of 2.4×10^{-4} cm².

2.6. Electrochemical measurements

The electrochemical analyses were performed using an Autolab electrochemical workstation (PGSTAT-100 potentiostat/galvanostat) connected to a personal computer that uses GPES electrochemical software.

The materials were mixed with acetylene black and PVDF at a mass ratio of 80 : 10 : 10 in ethanol and deposited on a nickel foam electrode. The as-prepared nickel foam electrodes were dried overnight at 70 °C and pressed. Each working electrode contained about 1 mg of electroactive material and had a geometric surface area of about 1 cm². A typical three-electrode experimental cell equipped with a stainless steel plate having 4 cm² of surface area as the counter electrode and a Metrohm Ag/AgCl (3 M KCl) as the reference electrode were used for the electrochemical characterization of the materials trapped by working electrodes.

The electrochemical measurements were carried out in aqueous 6 M KOH solutions as the electrolyte. Ultrapure water was obtained from Milli-Q equipment. The specific capacitance (C) was calculated from the cyclic chronopotentiometric curves according to eqn (1):

$$C = I\Delta t/m\Delta V \qquad (1)$$

where I is the charge/discharge current, Δt is the time for a full charge or discharge, m is the mass in grams of the active material in the electrode layer, and ΔV is the voltage change after a full charge or discharge.

Electrochemical impedance spectroscopy measurements were carried out by applying an AC amplitude of 10 mV in the frequency range of $0.01–10^6$ Hz at an open circuit potential with the help of an impedance spectrum analyser (GAMRY interface 1000 potentiostat). The electrochemical cell was placed in a Faradaic cage. Data were analysed with the help of Gamry Echem Analyst v. 6.03 software.

3. Results and discussion

The synthesis of carbon spheres was achieved by means of a catalytic CVD process at 900 °C using NiFe-LDHs as catalytic precursors and ethylene as a carbon source for a period of 60 min. After the CVD process, a black solid with metallic brilliance was formed using a quartz tube. The sample was collected from the inner part of the quartz reactor, powdered and submitted to a subsequent annealing process at 800 °C under an inert atmosphere in order to eliminate possible organic impurities. The final product was a black powder light in weight, hereinafter named as CS. Further characterization of pristine spheres is depicted in the ESI† (see SI 1).

As recently reported by our group, NiFe-LDHs are excellent catalysts for the synthesis of carbon nanoforms.[26,28] Moreover, we have demonstrated that the calcinated NiFe-LDH preserves the structural integrity, with the *in situ* formed FeNi₃ nanoparticles being the main catalytic seeds.[27] Herein, control experiments consisting of the calcination of NiFe-LDHs at 900 °C, supplying H₂ but in the

absence of a carbon source, gave rise to a mixture of $NiFe_2O_4$, NiO and $FeNi_3$ phases as revealed by XRPD (see SI 2.1, ESI†). However, further experiment with neither H₂ nor ethylene depicted the presence of only a mixture of $NiFe_2O_4$ and NiO, concluding that the $FeNi_3$ alloy is the active catalytic species in the CVD reaction, responsible for the growth of carbon nanoforms. Indeed, a low-temperature CVD process at 550 °C with bulk samples leads to a mixture of carbon nanoforms formed by few-layer graphene, carbon fibers and multi-wall carbon nanotubes (see ref. 28 for further information). According to Li and co-workers, these graphitic structures could evolve towards the formation of carbon spheres for larger times of feeding.[33] Herein, the presence of the catalyst is reflected in a decrease in the starting synthesis temperature towards *ca.* 800 °C, allowing the gram-scale formation of monodisperse CS (*vide infra*). In contrast, carbon sphere control experiments without the presence of a catalyst leads to an increase in the temperature to 900 °C yielding a lower amount of CS with a wide range of dimensions and morphologies, highlighting the crucial role of NiFe-LDHs (Fig. SI 2.2, ESI†).[34]

Inagaki[6,7] reported that the most probable mechanism for the formation of carbon spheres consists of the dissociation of ethylene (carbon source) at 900 °C into C and H. After that C starts to polymerize forming the so-called basic structural units (BSUs), whilst methane and hydrogen are also formed. Usually, the arrangement of these BSUs leads to three different textures in these carbon forms: concentric, radial and random.[7] The final disposition of these units depends on the precursor, heating treatment, feeding time and the interface between the carbon atoms and their surroundings during the thermal process.[7,35,36] Anyway, the exact role of the catalyst in the formation of spheres mediated by CVD procedures is not yet fully revealed. It seems that the FeNi₃ catalyst may act as a template, providing nucleation sites for the subsequent formation of spheres. Another possibility is its role in the modification and deposition of carbon radicals which are formed in the gas phase, *i.e.*, helping the decomposition of the carbon source instead of the polymerization reaction.[9]

The XRPD spectrum in CS was recorded in order to study the graphitic structure of the sample. Fig. 1A exhibits the presence of a main peak centred at *ca.* 25° and a secondary peak at *ca.* 43.8°, related to the (002) and the (100) planes of graphite, respectively. The common broadness of the peaks in the carbon sphere spectra indicates a low range in the structural order.[10,28] According to Bragg's equation, the interlayer spacing d_{002} of our CS is 0.356 nm, which agrees with the literature,[30,31] with a low deviation for the ideal d_{002} space (0.343 nm) in a graphitic structure (JCPDS-ICDD Card No. 41-1487). This value is intermediate between those measured for a carbon fiber (d_{002} = 0.342) and activated carbon atoms (d_{002} = 0.363), which is indicative of a relatively well-organised carbon structure.[5]

Raman spectra have been recorded to disclose the graphitic ordering of CS. Fig. 1B shows a representative Raman spectrum with the characteristic D and G bands centred at 1354 cm⁻¹, and 1590 cm⁻¹, respectively. The D band is related to the defects and disorder-induced modes, and the G band is associated with
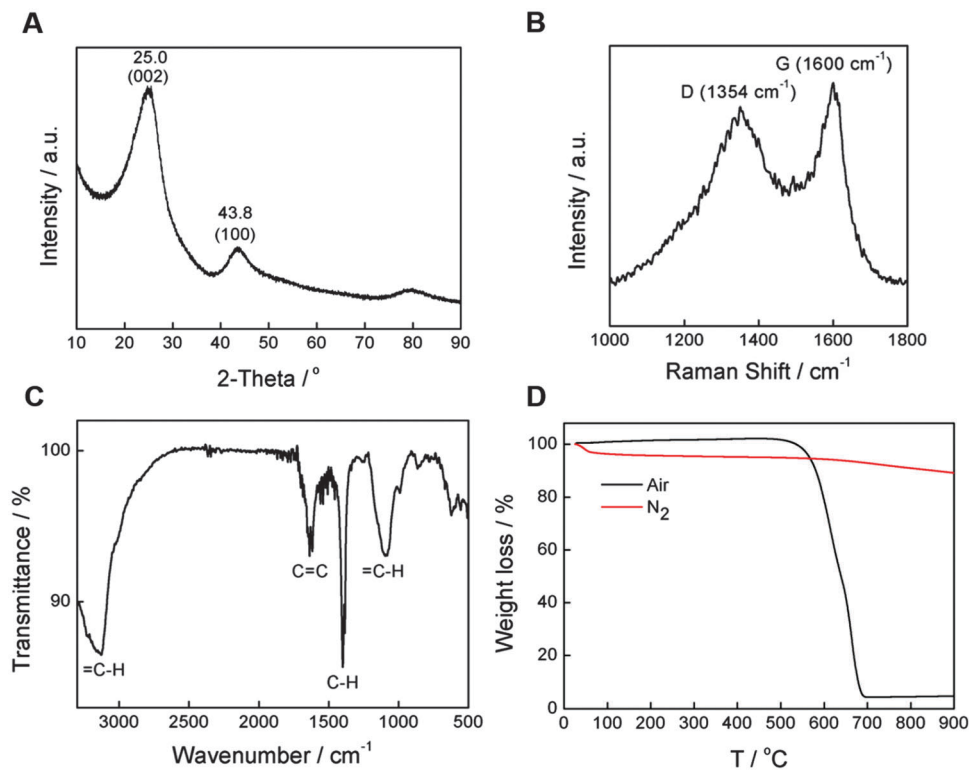
442 | *J. Mater. Chem. C*, 2016, **4**, 440–448

This journal is © The Royal Society of Chemistry 2016

Fig. 1 (A) XRPD, (B) Raman and (C) FT-IR spectra of CS. (D) TGA of CS in air (black line) and a nitrogen atmosphere (red).

the in-plane E_{2g} zone-centre mode, *i.e.* the vibration of sp^2-bonded carbon atoms in a two-dimensional hexagonal lattice. The I_D/I_G ratio is related to graphitic ordering in carbon materials, and a high I_D/I_G ratio involves a low degree of graphitization (order) in the carbon system, and *vice versa*. In our sample we measured a I_D/I_G ratio of *ca.* 0.80, showing a higher degree of graphitization (lower I_D/I_G) than most of the other CVD carbon spheres reported to date.[10,33,37,38] Lower I_D/I_G ratios can be achieved in the presence of MnO$_2$ or Ni doping.[39,40] In any case, our results are in accordance with the graphitization trend reported by Nieto-Márquez *et al.*: graphite > carbon nanotubes/nanofibers > carbon nanospheres > activated carbon.[10] A further comparison of all the synthesized spheres in this work can be found in SI 3 (ESI†).

FT-IR (Fig. 1C) confirmed the presence of C=C (1637 cm^{-1}) and =C–H groups (3100 and 1080 cm^{-1}, stretching and bending modes, respectively) in the CS, supporting the presence of an sp^2 structure. Among these, another band at *ca.* 1400 cm^{-1} can be found, related to the C–H bending mode.[34]

Furthermore, thermogravimetric analysis (TGA) and differential thermal analysis (DTA) experiments in air and under a N$_2$ atmosphere up to 900 °C were carried out. The thermogravimetric profile reveals that CS are stable in air below 530 °C; at *ca.* 560 °C they exhibit an abrupt mass loss of *ca.* 95% which ended at 700 °C (Fig. 1D). According to Serp *et al.* classification of carbon nanoforms based on the maximum of the gasification rate,[5] our sample is located in the range of carbon nano-spheres with a combustion temperature of *ca.* 630 °C depicted in the DTA (see SI 4, ESI†). In turn, the experiment in N$_2$ exhibits a stable thermal behaviour, showing only a weight loss of *ca.* 10% when 900 °C is reached. It is

worth noting that in the presence of air, a slight increase of mass (*ca.* 105%) is observed just before thermal decomposition; this is attributed to the oxidizing process of graphitic flakes into oxidized graphite. In contrast, this effect is not seen in N$_2$.[34,41]

After studying the structural properties of the spheres, their morphology was unveiled by means of FESEM and HRTEM, depicting the spherically characteristic shape of CS, with a large quantity of them usually forming aggregates (Fig. 2). The accretion of spheres into clusters of several microns (see SI 5, ESI†) was described by Kroto *et al.* for feeding times higher than 10 min,[34] or by Pol and co-workers as a result of cooling the system from high temperature to room temperature.[35] Anyway, it is worth noting that this coalescence is related to the presence of reactive dangling bonds on the surface, which gives them a high surface reactivity.[4,10] Indeed, the EDAX analysis of the sample revealed a carbon content of 93.2 atomic% and an oxygen content of 6.8%. These results are corroborated by C, H, N elemental analysis, with a carbon content of 93.3% (atomic ratio) and 0.4% of H. No N was detected. Atomic percentages were also confirmed by XPS (see SI 6.1, ESI†). Furthermore, the XPS spectrum of C$_{1s}$ clearly exhibits a main peak which can be deconvoluted into sp^2 and sp^3 components. No trace of the catalyst (Ni and Fe) was found in the spectra of the CS (SI 6.2, ESI†). Finally, the synthesis of carbon spheres at a higher temperature (1000 °C) depicted a decrease of *ca.* 1% in the O atomic percentage (a decrease of *ca.* 11% of the total oxygen content). The N signal remains residual (SI 6.1, ESI†).

The particle size distribution was determined by measuring 50 spheres in the SEM images, giving rise to an average diameter of 740 ± 42 nm. This is in sharp contrast with the

This journal is © The Royal Society of Chemistry 2016

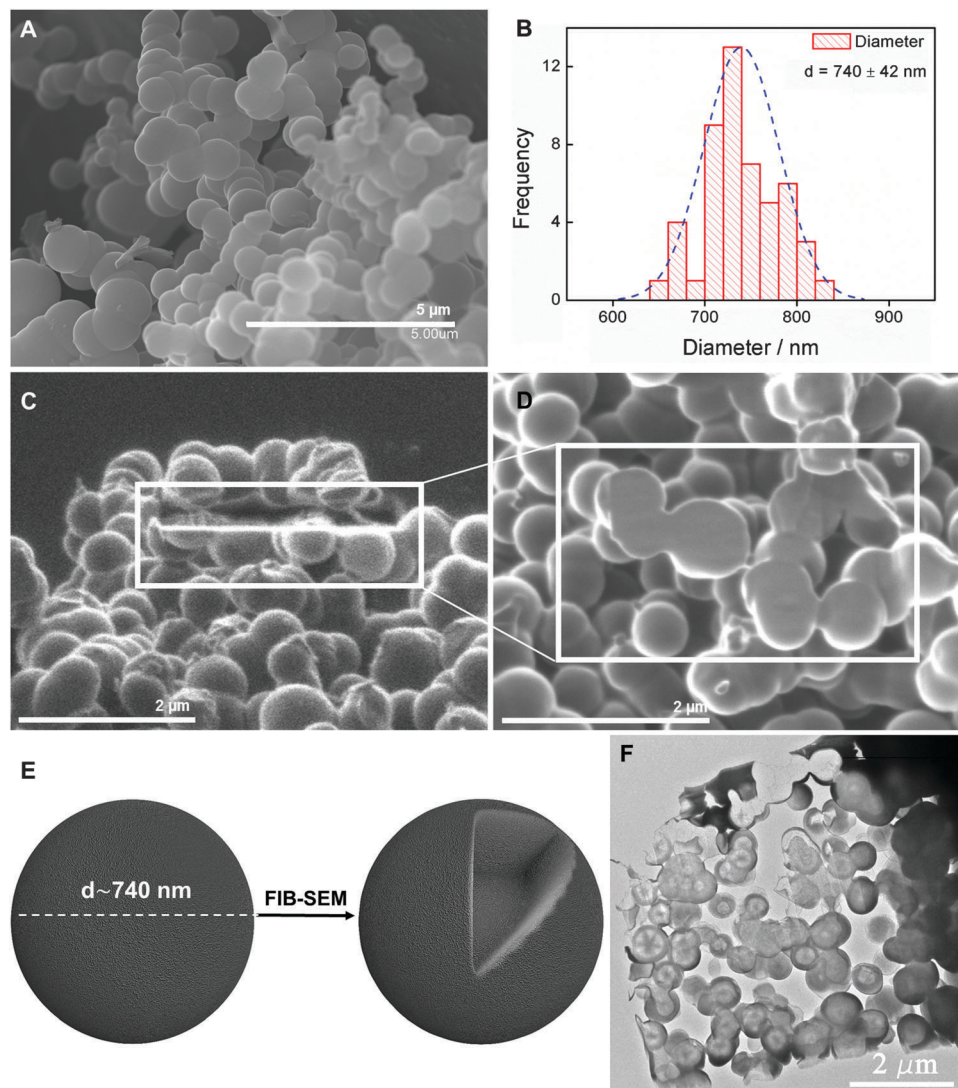*J. Mater. Chem. C*, 2016, **4**, 440–448 | **443**

Fig. 2 (A) FESEM image of CS. (B) Histogram displaying the average diameter taken from FESEM images. (C) FIB-SEM image of the milled region, it is remarked within the white square. (D) FIB-SEM cross-section image of the same region of (C) depicting a solid inner structure. (E) Idealized 3D representation of a sphere before and after the FIB, highlighting the solid inner structure. (F) Bright field TEM image of electron-transparent lamella prepared by FIB-SEM. The porosity between the carbon spheres can be clearly seen.

wide range of diameters obtained in the control experiments (see SI 2, ESI†), and highlights the role played by the NiFe-LDH catalytic precursor in controlling the size distribution of the spheres.

In order to determine directly whether the spheres are hollow or not, we have taken advantage of a dual beam focused ion beam-SEM instrument. Precise milling was carried out over several spheres. An example of a typical zone where the focused ion milling process has been applied is shown in Fig. 2C. The cross-section acquired after the milling process supplies detailed information of the specimen subsurface, highlighting the existence of a solid inner structure in the spheres, as depicted in Fig. 2D and E.

Furthermore, a lamella thinned down to electron-transparency has been studied by TEM showing the absence of mesopores and porosity between the carbon spheres (vide infra) (Fig. 2F). The preparation of these lamellae is detailed in SI 7 (ESI†).

HRTEM images displayed nearly perfect spherical morphologies with an average diameter of ca. 700–800 nm (Fig. 3A), disposed usually in a chain-like structure due to the accretion effect. These diameters are in good accordance with the value extracted from FESEM studies. A deeper look into their internal structure revealed a concentric arrangement of the graphitic planes (as demonstrated by HRTEM vide infra).[6] In addition, the distance between the graphitic planes also matches with that calculated from Bragg's equation according to the XRPD spectrum (vide supra).

Interestingly, these chain-like structures can be disassembled by sonication, obtaining relatively stable suspensions of CS exhibiting the characteristic Tyndall–Faraday effect. Concretely, by suspending the powder in toluene (1 mg of CS in 10 mL) and submitting it to bath sonication for 30 min, almost all of the aggregates can be individualized. Fig. 3B and C depict an HRTEM image showing the presence of isolated and monodisperse spheres, retaining their

444 | J. Mater. Chem. C, 2016, 4, 440–448

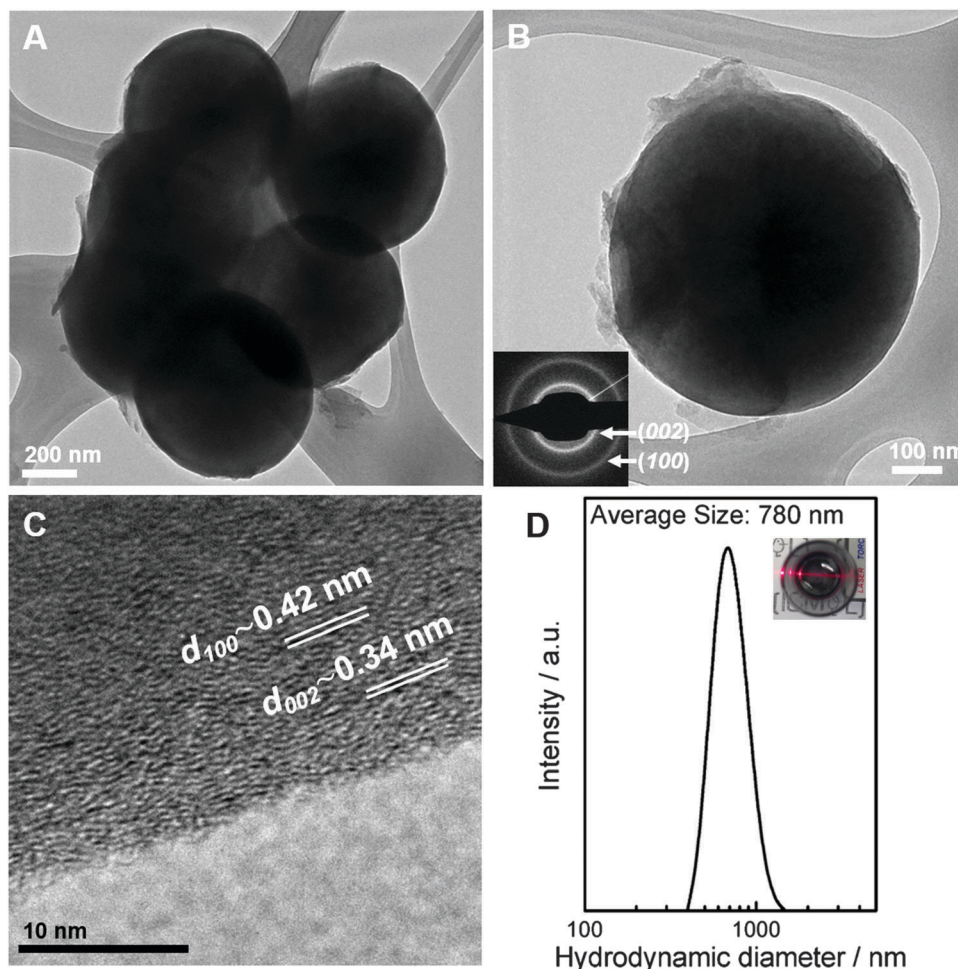This journal is © The Royal Society of Chemistry 2016

Fig. 3   HRTEM image depicting (A) a cluster of spheres, disposed in a chain-like structure, and (B) a single sphere from the CS sample after a sonication procedure in toluene. The inset in (B) shows the selected area electron diffraction (SAED) pattern displaying two rings corresponding to (002) and (100) planes. (C) High magnification image of the interface from a single sphere, highlighting the (002) and (100) planes and the distance between crystallographic lattices (D). Distribution of sizes extracted from DLS measurements for CS. Its inset shows the visible Tyndall–Faraday effect, resulting from the scattering of the irradiated beam by the particles in a toluene solution.

intrinsic structure. In their spherical surface, some broken edges can be seen, due to the disaggregation of the clusters after the sonication process. Furthermore, Dynamic Light Scattering (DLS) was carried out with this suspension, in order to further study the size distribution of the sample (Fig. 3D), as well as the possible presence of bigger clusters. We observed that the average hydrodynamic diameter – a complex function that describes a Gaussian distribution – is centred at *ca.* 780 nm, in good agreement with the electron microscopy observations and the classification proposed by Serp *et al.*[5]

In order to determine the surface texture of the spheres, N_2 adsorption–desorption isotherms were measured. The CS showed a BET surface area value of 16.2 m^2 g^{-1}, indicative of the absence of mesoporosity on its surface, in accordance with previously published studies.[10] In contrast, carbon spheres with a mesoporous structure depicted larger BET surface areas of *ca.* 1400–1600 m^2 g^{-1}.[36,37] It is worth saying that this value is slightly higher than that exhibited by the pristine spheres (3.6 m^2 g^{-1}), as a consequence of annealing. In line with that,

differential pore volume distribution of the spheres by DFT has been calculated, suggesting the presence of ultramicropores (see SI 8, ESI†).[42–44]

One of the most important fields of application of CS and related nanomaterials is the energy storage and conversion.[45,46] Among others, supercapacitors (SCs) are attracting increasing attention due to their potential to deliver high power densities in short periods of time with high cyclability and durability.[47] In this sense, the graphitic character, porosity, conductivity or the presence of oxygen functionalities could greatly affect the properties of SCs, providing us with important information about the presence of oxygen functionalities on the surface.

For comparative purposes, we have tested the electrochemical properties of the CS as electrode materials for SCs in a conventional three-electrode cell. The powdered sample was mixed with acetylene black and poly-vinylidene fluoride at a mass ratio of 80:10:10 with ethanol. The mixture was cast on a 1 cm^2 Ni-foam collector, dried and pressed to minimize the loss of the active material during electrochemical testing. The electrochemical properties

were measured by means of cyclic voltammetry (CV) using 6 M KOH (99.99%) as the electrolyte in an applied voltage range of of 0 to −1 V (*vs.* Ag/AgCl). Fig. 4A shows the quasi-rectangular cyclic voltammograms recorded at different scan rates, in which the large areas suggest an appropriate supercapacitive behaviour, although these CS are not porous, indicative of an activated surface.[48] Moreover, galvanostatic charge–discharge cycling was also measured in order to study the specific capacitance of these CS (Fig. 4B). A relatively large discharge capacity of *ca.* 132 F g^{−1} was obtained for a current density of 1 A g^{−1} (inset in Fig. 4B), overpassing that recently reported for related microporous CS,[49] a clear indication of the improved graphitic quality of the as-synthesized materials and the presence of an oxidized shell in accordance with the EDAX and elemental analysis results (*vide supra*). Because the oxygen content has a close relationship with carbonization temperature, the electrochemical properties of CS synthesized at 1000 °C were measured, exhibiting lower values of capacitances as seen in SI 9 (ESI†). This fact can be related to the minor presence of oxygen on the surface of those spheres, as revealed by XPS (SI 6.1, ESI†).

The potential electrochemical impedance spectroscopy (EIS) shows Nyquist plots with a nearly vertical line, typical of capacitive behaviour. In the inset of Fig. 4 a minor increase in the imaginary part can be seen due to electrolyte resistance. The corresponding conductance shows a typical behaviour, with values close to zero at low frequencies increasing with the increasing frequency, with a maximum of 1.3 S.[50]

A complete physical characterization of CS has been done measuring the transport properties using the four-probe method. The CS exhibited a nonmetallic behaviour as can be observed in the thermal evolution of resistance (Fig. 5). Fig. 5 shows characteristic non-linear and symmetrical I–V curves for the whole studied temperature range. The non-linearity increases when the temperature is reduced, observing semiconductor behaviour. The electrical conductivity at room temperature is 1.92×10^{-2} S cm^{−1} and it is reduced by four orders of magnitude when the temperature decreases, which is 1.32×10^{-6} S cm^{−1} at 2 K (Fig. 5). Furthermore, the conductivity matches perfectly with other values reported in the literature for CS.[16,17]

Studies dealing with the electrical properties of CS are very scarce. To the best of our knowledge, the first work that has measured the electrical properties of the CS is from Coville *et al.*,[16,17] where they studied the electrical transport mechanisms in nitrogen and boron-doped carbon spheres. These studies show that the dominant conduction mechanism in pristine CS is Mott variable range hopping (Mott VRH). In our case, this model provides a good description of the thermal dependence of electrical conductivity in the 300–2 K temperature range (Fig. SI 10, ESI†). Thus, the experimental behaviour is well fitted by the expression $\sigma(T) = \sigma_0 \cdot \exp[-(T_0/T)^n]$, with $n = 1/4$. The VRH model of conductivity represents a phonon-assisted mechanism of charge transport and it is normally associated with amorphous semiconductors, semiconductor glasses[51,52] and more recently with amorphous carbon.[17]
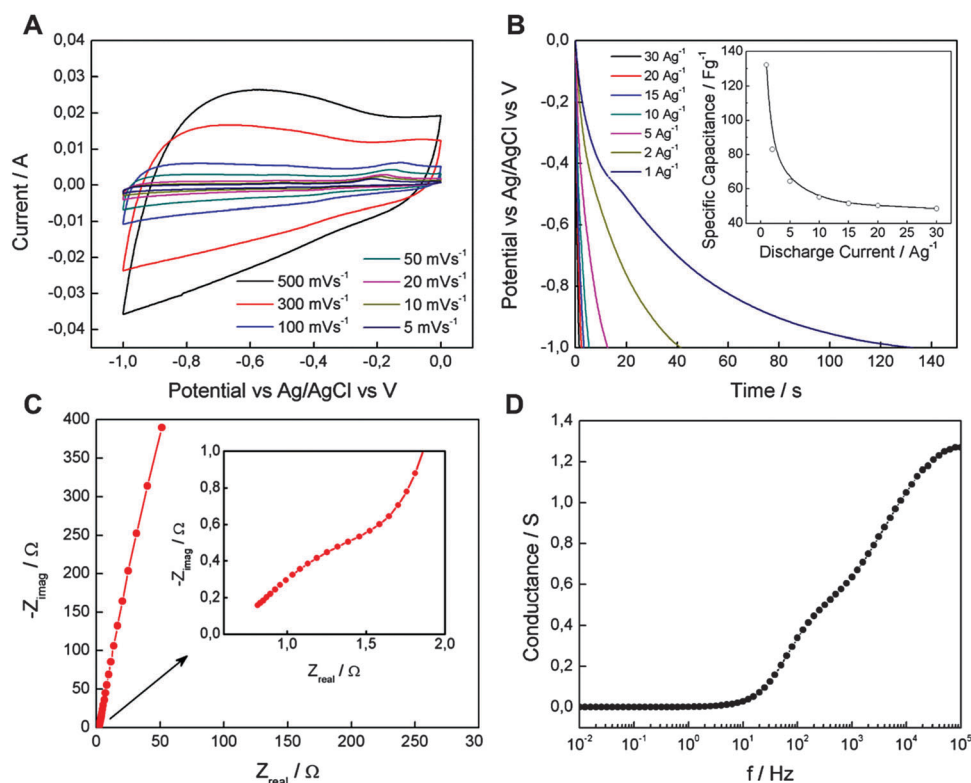

Fig. 4 Electrochemical properties of CS. (A) CV curve at various scan rates in a 6 M KOH aqueous solution. (B) Galvanostatic discharge curves at different discharge current densities. The inset represents the specific capacitance of the material at different discharge current densities. Electrochemical impedance spectra of CS in a 6 M KOH electrolyte. (C) Nyquist plots and (D) the response of conductance at different frequencies. The inset shows the high-frequency region.
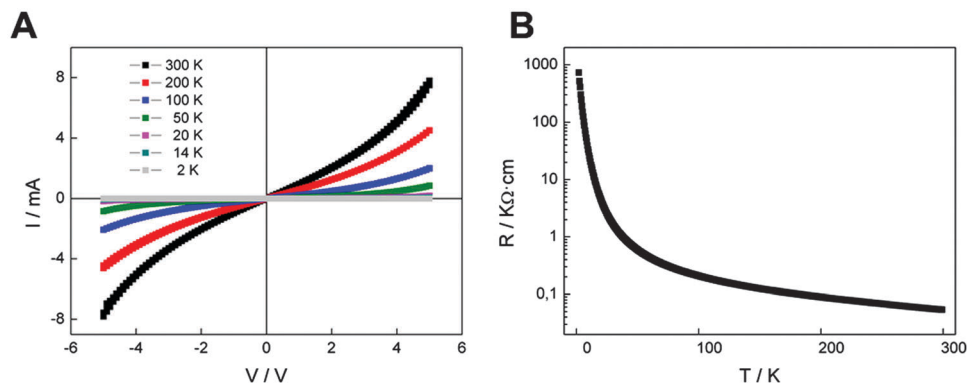
Fig. 5 (A) I–V curves for a temperature range from 300 K to 2 K. The electrical conductivity at room temperature is 1.92×10^{-2} S cm^{-1}. (B) Thermal resistance dependence of the CS.

We also measured the magnetoresistance (MR) properties of CS in the applied fields of 8 T in a PPMS system, revealing an intrinsic magnetoresistance (MR) of *ca.* 72% at low temperatures (Fig. 6). MR is calculated as MR (%) = $[R(H) - R(0)/R(0)] \times 100$, where $R(H)$ is the resistivity under the magnetic field B and $R(0)$ is the resistivity without any magnetic field. As long as we increase the temperature, the MR falls dramatically until no signal is observed above 100 K.

Fig. 6 shows a positive and non-saturated MR that decreases dramatically when the temperature increases for all the temperature range studied (from 50 K to 2 K). This positive, non-saturated MR behavior has also been found for other crystalline and amorphous nanocarbons and carbon composites.[20–25] All the experimental data of the Fig. 6 were fitted with the relation of MR $\propto (\mu_0 \cdot \mu \cdot |H|)^2$ (Fig. SI 10, ESI†). The quadratic term is related to the ordinary MR (OMR)[20] due to the curving of electron trajectories in the carbon plane, which results in a positive MR, and has a quadratic magnetic dependence of MR $\propto (\mu_0 \cdot \mu \cdot |H|)^2$, where μ is mobility.[20–24] The magnetic measurements revealed a very small magnetic phase in the CS (Fig. SI 11, ESI†). This magnetic phase probably comes from a small rest of the catalyst. However, the XPS analysis of CS showed the absence of the catalyst on the sample surface, highlighting the residual character of the catalyst present in the CS (Fig. SI 6.2, ESI†). Therefore, the influence of the magnetic rest of the catalyst in the MR is very weak, and almost negligible.
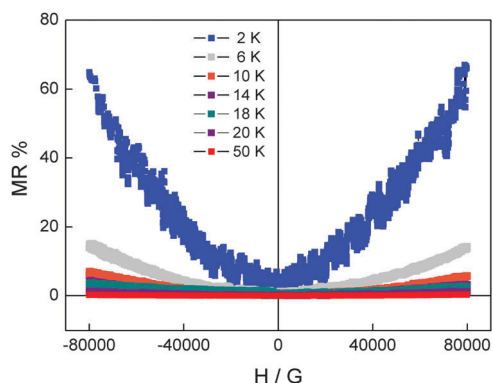
Finally, the dramatic temperature dependence of the MR (Fig. SI 12, ESI†) is an indication of the predominant contribution of the OMR to the MR observed in the CS. These results pave the way for using CS not only as a reinforcing agent of polymers, but also as electronically active building blocks in the design of hybrid multifunctional composites.

4. Conclusions

Carbon spheres with a diameter of *ca.* 740 nm have been synthesized in gram-scale proportions by means of a CVD method using NiFe-LDHs as catalyst precursors. Control experiments revealed that the presence of the FeNi$_3$ catalyst allows us to control the size distribution, giving rise to a monodisperse sample. XRPD and Raman spectroscopy demonstrate their graphitic nature, with an I_D/I_G ratio of *ca.* 0.80, therefore exhibiting a higher degree of graphitization than other spheres reported to date. Moreover, these CS can be individualized in toluene by means of sonication, beating the accretion effects. Furthermore, FIB-SEM experiments show that the inner structure of the spheres is solid and consists of concentric graphitic planes. Concerning their surface properties, nitrogen adsorption, XPS and electrochemical testing revealed the presence of redox functionalities on their surface behaving as appropriated electrode materials for supercapacitors despite their intrinsic non-mesoporous nature.

Finally, their transport properties have also been studied, exhibiting a semiconducting behaviour at low temperatures and a giant magnetoresistance of *ca.* 72% at 2 K and a voltage of 3 V. The MR was strongly dependent on the temperature and principally has a quadratic dependence, following an ordinary MR behaviour. These CS are promising candidates for polymer reinforcement and as building blocks for preparing more complex hybrid composites.

Acknowledgements

Fig. 6 MR dependence on the temperature of the CS.

References

1 H. W. Kroto, J. R. Heath, S. C. O'Brien, R. F. Curl and R. E. Smalley, *Nature*, 1985, **318**, 162–163.

2 J. L. Delgado, M. Herranz and N. Martín, *J. Mater. Chem.*, 2008, **18**, 1417–1426.

3 A. W. Francis, *Ind. Eng. Chem.*, 1931, **23**, 612–617.

4 Z. C. Kang and Z. L. Wang, *J. Phys. Chem.*, 1996, **100**, 5163–5165.

5 P. Serp, R. Feurer, P. Kalck, Y. Kihn, J. L. Faria and J. L. Figueiredo, *Carbon*, 2001, **39**, 621–626.

6 M. Inagaki, *Solid State Ionics*, 1996, **86**, 833–839.

7 M. Inagaki, *Carbon*, 1997, **35**, 711–713.

8 Y. Xia, B. Gates, Y. Yin and Y. Lu, *Adv. Mater.*, 2000, **12**, 693–713.

9 A. A. Deshmukh, S. D. Mhlanga and N. J. Coville, *Mater. Sci. Eng., R*, 2010, **70**, 1–28.

10 A. Nieto-Márquez, R. Romero, A. Romero and J. L. Valverde, *J. Mater. Chem.*, 2011, **21**, 1664–1672.

11 *Carbon materials for catalysis*, ed. P. Serp and J. L. Figueiredo, John Wiley & Sons, Hoboken, N.J, 2009.

12 N. Fleischer, M. Genut and A. Gorodnev, *Am. Ceram. Soc. Bull.*, 2006, **85**, 27–28.

13 X. He, F. Wu and M. Zheng, *Diamond Relat. Mater.*, 2007, **16**, 311–315.

14 Y. Z. Jin, Y. J. Kim, C. Gao, Y. Q. Zhu, A. Huczko, M. Endo and H. W. Kroto, *Carbon*, 2006, **44**, 724–729.

15 F. P. Hu, Z. Wang, Y. Li, C. Li, X. Zhang and P. K. Shen, *J. Power Sources*, 2008, **177**, 61–66.

16 W. P. Wright, V. D. Marsicano, J. M. Keartland, R. M. Erasmus, S. M. A. Dube and N. J. Coville, *Mater. Chem. Phys.*, 2014, **147**, 908–914.

17 K. C. Mondal, A. M. Strydom, Z. Tetana, S. D. Mhlanga, M. J. Witcomb, J. Havel, R. M. Erasmus and N. J. Coville, *Mater. Chem. Phys.*, 2009, **114**, 973–977.

18 Y. Z. Jin, C. Gao, H. W. Kroto and T. Maekawa, *Macromol. Rapid Commun.*, 2005, **26**, 1133–1139.

19 H. Ismail, P. K. Freakley and E. Sheng, *Eur. Polym. J.*, 1995, **31**, 1049–1056.

20 H. Gu, X. Zhang, H. Wei, Y. Huang, S. Wei and Z. Guo, *Chem. Soc. Rev.*, 2013, **42**, 5907–5943.

21 C. Bosch-Navarro, F. Busolo, E. Coronado, Y. Duan, C. Martí-Gastaldo and H. Prima-Garcia, *J. Mater. Chem. C*, 2013, **1**, 4590–4598.

22 J. Wang, X. Zhang, C. Wan, J. Vanacken and V. V. Moshchalkov, *Carbon*, 2013, **59**, 278–282.

23 Z.-M. Liao, H.-C. Wu, S. Kumar, G. S. Duesberg, Y.-B. Zhou, G. L. W. Cross, I. V. Shvets and D.-P. Yu, *Adv. Mater.*, 2012, **24**, 1862–1866.

24 Y.-B. Zhou, B.-H. Han, Z.-M. Liao, H.-C. Wu and D.-P. Yu, *Appl. Phys. Lett.*, 2011, **98**, 222502.

25 J. Zhu, Z. Luo, S. Wu, N. Haldolaarachchige, D. P. Young, S. Wei and Z. Guo, *J. Mater. Chem.*, 2012, **22**, 835–844.

26 G. Abellán, C. Martí-Gastaldo, A. Ribera and E. Coronado, *Acc. Chem. Res.*, 2015, **48**, 1601–1611.

27 G. Abellán, E. Coronado, C. Martí-Gastaldo, A. Ribera and J. F. Sánchez-Royo, *Chem. Sci.*, 2012, **3**, 1481–1485.

28 G. Abellán, J. A. Carrasco, E. Coronado, J. P. Prieto-Ruiz and H. Prima-García, *Adv. Mater. Interfaces*, 2014, **1**, 1400184.

29 G. Abellán, J. G. Martínez, T. F. Otero, A. Ribera and E. Coronado, *Electrochem. Commun.*, 2014, **39**, 15–18.

30 G. Abellán, E. Coronado, C. Martí-Gastaldo, A. Ribera and T. F. Otero, *Part. Part. Syst. Charact.*, 2013, 853–863.

31 G. Abellán, E. Coronado, C. Martí-Gastaldo, E. Pinilla-Cienfuegos and A. Ribera, *J. Mater. Chem.*, 2010, **20**, 7451–7455.

32 R. Langford and C. Clinton, *Micron*, 2004, **35**, 607–611.

33 Y. Li, J. Chen, Q. Xu, L. He and Z. Chen, *J. Phys. Chem. C*, 2009, **113**, 10085–10089.

34 Y. Z. Jin, C. Gao, W. K. Hsu, Y. Zhu, A. Huczko, M. Bystrzejewski, M. Roe, C. Y. Lee, S. Acquah, H. Kroto and D. R. M. Walton, *Carbon*, 2005, **43**, 1944–1953.

35 V. G. Pol, M. Motiei, A. Gedanken, J. Calderon-Moreno and M. Yoshimura, *Carbon*, 2004, **42**, 111–116.

36 L. C. Yang, Y. Shi, Q. S. Gao, B. Wang, Y. P. Wu and Y. Tang, *Carbon*, 2008, **46**, 1816–1818.

37 A. Nieto-Márquez, D. Toledano, J. C. Lazo, A. Romero and J. L. Valverde, *Appl. Catal., A*, 2010, **373**, 192–200.

38 H. Qian, F. Han, B. Zhang, Y. Guo, J. Yue and B. Peng, *Carbon*, 2004, **42**, 761–766.

39 M. Liu, L. Gan, W. Xiong, Z. Xu, D. Zhu and L. Chen, *J. Mater. Chem. A*, 2014, **2**, 2555–2562.

40 M. Liu, L. Gan, W. Xiong, F. Zhao, X. Fan, D. Zhu, Z. Xu, Z. Hao and L. Chen, *Energy Fuels*, 2013, **27**, 1168–1173.

41 Y. J. Kim, M. I. Kim, C. H. Yun, J. Y. Chang, C. R. Park and M. Inagaki, *J. Colloid Interface Sci.*, 2004, **274**, 555–562.

42 W. Li, D. Chen, Z. Li, Y. Shi, Y. Wan, G. Wang, Z. Jiang and D. Zhao, *Carbon*, 2007, **45**, 1757–1763.

43 D. Fujikawa, M. Uota, T. Yoshimura, G. Sakai and T. Kijima, *Chem. Lett.*, 2006, **35**, 432–433.

44 M. Liu, J. Qian, Y. Zhao, D. Zhu, L. Gan and L. Chen, *J. Mater. Chem. A*, 2015, **3**, 11517–11526.

45 M. Liu, X. Ma, L. Gan, Z. Xu, D. Zhu and L. Chen, *J. Mater. Chem. A*, 2014, **2**, 17107–17114.

46 D. Zhu, Y. Wang, L. Gan, M. Liu, K. Cheng, Y. Zhao, X. Deng and D. Sun, *Electrochim. Acta*, 2015, **158**, 166–174.

47 F. Beguin and E. Frackowiak, *Supercapacitors: Materials, Systems and Applications*, John Wiley & Sons, 2013.

48 X. Ma, L. Gan, M. Liu, P. K. Tripathi, Y. Zhao, Z. Xu, D. Zhu and L. Chen, *J. Mater. Chem. A*, 2014, **2**, 8407–8415.

49 W. Yang, Y. Feng, D. Xiao and H. Yuan, *Int. J. Energy Res.*, 2015, **39**, 805–811.

50 Y. Gao, Y. S. Zhou, M. Qian, X. N. He, J. Redepenning, P. Goodman, H. M. Li, L. Jiang and Y. F. Lu, *Carbon*, 2013, **51**, 52–58.

51 N. F. Mott, *Philos. Mag.*, 1969, **19**, 835–852.

52 N. F. Mott and M. Kaveh, *Adv. Phys.*, 1985, **34**, 329–401.

448 | *J. Mater. Chem. C*, 2016, **4**, 440–448

This journal is © The Royal Society of Chemistry 2016